Jun Cai*, Kuaishe Wang and Yingying Han

A Comparative Study on Johnson Cook, Modified Zerilli–Armstrong and Arrhenius-Type Constitutive Models to Predict High-Temperature Flow Behavior of Ti–6Al–4V Alloy in α + β Phase

Abstract: True stress and true strain values obtained from isothermal compression tests over a wide temperature range from 1,073 to 1,323 K and a strain rate range from 0.001 to 1 s^{-1} were employed to establish the constitutive equations based on Johnson Cook, modified Zerilli–Armstrong (ZA) and strain-compensated Arrhenius-type models, respectively, to predict the high-temperature flow behavior of Ti–6Al–4V alloy in α + β phase. Furthermore, a comparative study has been made on the capability of the three models to represent the elevated temperature flow behavior of Ti–6Al–4V alloy. Suitability of the three models was evaluated by comparing both the correlation coefficient R and the average absolute relative error (AARE). The results showed that the Johnson Cook model is inadequate to provide good description of flow behavior of Ti–6Al–4V alloy in α + β phase domain, while the predicted values of modified ZA model and the strain-compensated Arrhenius-type model could agree well with the experimental values except under some deformation conditions. Meanwhile, the modified ZA model could track the deformation behavior more accurately than other model throughout the entire temperature and strain rate range.

Keywords: Ti–6Al–4V alloy, hot compression deformation, constitutive equation, flow stress

DOI 10.1515/htmp-2014-0157
Received September 12, 2014; accepted March 10, 2015

***Corresponding author: Jun Cai,** School of Metallurgical Engineering, Xi'an University of Architecture and Technology, Xi'an 710055, China, E-mail: jeffreycai0116@gmail.com
Kuaishe Wang, School of Metallurgical Engineering, Xi'an University of Architecture and Technology, Xi'an 710055, China
Yingying Han, Beijng North Vehicle Group Corporation, Beijing 100072, China

Introduction

With the development of numerical simulation method, finite element method (FEM) has been widely and successfully used for analysis of various metal forming processes and optimization of the hot formation process parameters [1, 2]. Constitutive equation which represents the flow behavior of materials is used as input to the FEM code for simulating the materials deformation behaviors under specified loading conditions [3–5]. Therefore, the accuracy of the simulation results largely depends on how accurately the deformation behavior of the material is represented by the constitutive equation [6, 7].

For the past few years, many constitutive models have been proposed or modified to describe the flow behavior. Among these models, Johnson Cook model has been successfully incorporated in FEM to describe the hot deformation behavior of alloys due to its simple multiplication form [6, 7]. The Johnson Cook model involves only five material constants which are determined normally by experiment [8]. And due to the advantages of simple form, small calculation quantity and rapid calculation speed, Johnson Cook model has been widely applied in various kinds of commercial FEM software to describe the high-temperature deformation behavior of alloys [9]. The Zerilli–Armstrong (ZA) model is also very useful because it considers coupled strain and temperature effects. This model has been used to analyze different face-centered cubic and body-centered cubic materials over different strain rates at temperatures between room temperature and 0.6 T_m (T_m is the melting point) [10, 11]. Samantaray et al. [12] proposed a modified ZA model by considering the effects of thermal softening, strain rate hardening and isotropic hardening as well as the coupled effects of temperature, strain and strain rate on flow stress and accurately describe the elevated temperature flow behaviors of modified 9Cr–1Mo steel and type 316L(N) steel using this model. And Zhang et al. [13] employed modified ZA model to predict the flow behavior of alloy IC10 over a wide range of temperatures and strain

rates. Meanwhile, the hyperbolic sine Arrhenius-type constitutive model has been successfully applied to predict the elevated temperature flow behavior of materials. Then a strain-dependent parameter was introduced into the Arrhenius-type model to predict the flow stress of metallic materials [14–16].

As a kind of α + β-type titanium alloy, Ti–6Al–4V alloy is one of the most important and widely used titanium alloys in the aerospace industry, which has low density and attractive mechanical and corrosion-resistant properties. Therefore, great attention has been given in the scientific literature to the investigation of the deformation behavior of this alloy [17, 18]. As is well known, the deformation behavior of Ti–6Al–4V alloy is sensitive to the processing parameters such as temperature and strain rate [19], and a lot of hot forming process of Ti–6Al–4V alloy is located at α + β phase [20–22]. Hence, a thorough study on elevated temperature deformation behavior of Ti–6Al–4V alloy is significant to properly design the deformation parameters.

The objective of this study is to establish the suitable constitutive equations based on modified Johnson Cook, modified ZA and strain-compensated Arrhenius-type models, respectively, to predict the evaluated temperature flow stress of Ti–6Al–4V alloy in α + β phase region and make a comparative study on their capability to predict the elevated temperature flow behavior. For this purpose, isothermal hot compression tests were conducted in the temperature range of 1,073–1,223 K and strain rates range of 0.001–1 s^{-1}. The experimental stress–strain data were then employed to derive the modified Johnson Cook, modified ZA and strain-compensated Arrhenius-type models constitutive equation. Finally, the suitability of these three models was evaluated by comparing the correlation coefficient (R) and average absolute relative error (AARE).

Experimental procedure

Commercial Ti–6Al–4V alloy was used for the hot compression test. The chemical composition is shown in Table 1. Cylindrical specimens with a diameter of 8 mm and a height of 12 mm were prepared for hot compression tests, as shown in Figure 1. In order to obtain the heat balance, each specimen was heated to the deformation temperature at a rate of 10°C/s, and held for 5 min at the isothermal conditions before compression tests. Then isothermal compression tests were carried out in the strain rate range of 0.001–1 s^{-1} and the temperatures range of 1,073–1,223 K by Gleeble-3500 simulator. After deformation, the specimens were quenched in water, and the strain–stress curves were recorded automatically during isothermal compression process.

Table 1: Chemical composition of as-received Ti–6Al–4V billet.

Main component (wt%)			Impurities (wt%)			
Al	V	Ti	Fe	C	H	O
6.02	3.78	Balance	0.08	0.007	0.0082	0.074

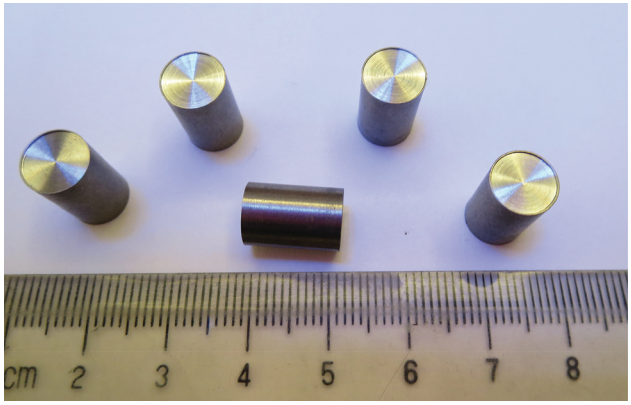

Figure 1: Typical appearance of the Ti–6Al–4V alloy specimens.

Results and discussion

Johnson Cook model

The Johnson Cook model is expressed as follows [23]:

$$\sigma = (A + B\varepsilon^n)(1 + C\ \ln \dot{\varepsilon}^*)(1 - T^{*m}) \tag{1}$$

where σ is flow stress in MPa, ε is the true strain, $\dot{\varepsilon}^* = \dot{\varepsilon}/\dot{\varepsilon}_0$ is the dimensionless strain rate with $\dot{\varepsilon}$ being the strain rate (s^{-1}) and $\dot{\varepsilon}_0$ the reference strain rate (s^{-1}), A is the yield stress at reference temperature and strain rate, B is the coefficient of strain hardening, n is the exponent of strain hardening and T^* is homologous temperature and expressed as eq. (2):

$$T^* = \frac{T - T_{\text{ref}}}{T_{\text{m}} - T_{\text{ref}}} \tag{2}$$

where T is the current and reference temperatures (K), T_{m} is the melting temperature (1,903 K for Ti–6Al–4V alloy) and T_{ref} is the reference temperature ($T \geq T_{\text{ref}}$). C and m are the material constants that represent the coefficient of strain rate hardening and thermal softening exponent, respectively.

In present study, 1,073 K as well as 1 s^{-1} are taken as reference temperature and reference strain rate respectively. When the deformation temperature is 1,073 K and strain rate is 1 s^{-1}, eq. (1) can be written as

$$\sigma = A + B\varepsilon^n \tag{3}$$

The value of A is obtained from the yield stress of the flow curve at 1,073 K as well as 1 s^{-1} (276.53 MPa). Substituting the value of A and the corresponding experimental flow stress data into eq. (3), the relationship between $\ln(\sigma - A)$ and $\ln\varepsilon$ can be obtained. Figure 2 illustrates the relationship between $\ln(\sigma - A)$ and $\ln\varepsilon$ at 1,073 K and 1 s^{-1}. Then the values of B and n can be obtained from the fitting curve.

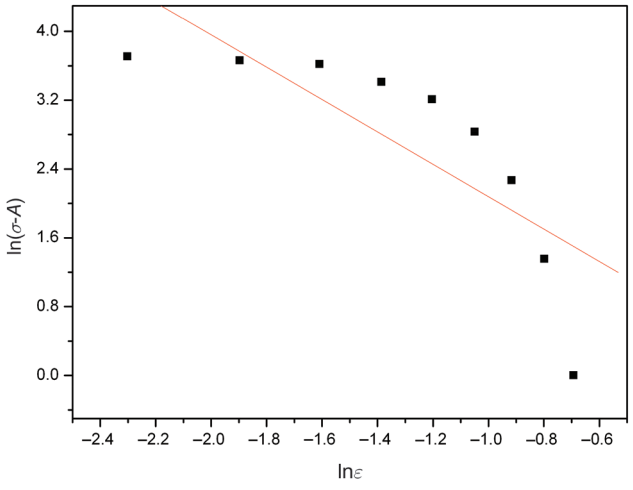

Figure 2: Relationship between $\ln(\sigma - A)$ and ε at 1,073 K and 1 s^{-1}.

When the deformation temperature is 1,073 K, eq. (1) can be changed into

$$\sigma = (A + B\varepsilon^n)(1 + C\ln\dot{\varepsilon}^*) \tag{4}$$

Therefore, the values of C can be obtained from the slope of the lines in $\sigma/A + B\varepsilon^n - \ln(\dot{\varepsilon}^*)$ plot. Figure 3 shows the variation of $\sigma/A + B\varepsilon^n$ with $\ln(\dot{\varepsilon}^*)$at the temperature of 1,073 K. Similarly, at reference strain rate, the flow stress would be independent from thermal softening term since $\ln(\dot{\varepsilon}^*) = 0$. Therefore, eq. (1) can be expressed as

$$\sigma = (A + B\varepsilon^n)(1 - T^*m) \tag{5}$$

Using the flow stress data for a particular strain at different temperatures, the relationship between $\ln[1 - \sigma/(A + B\varepsilon^n)]$ and $\ln T^*$ can be obtained. Then the values of m for eight different strains can be obtained from the slopes of the linear fitting curves, as shown in Figure 4.

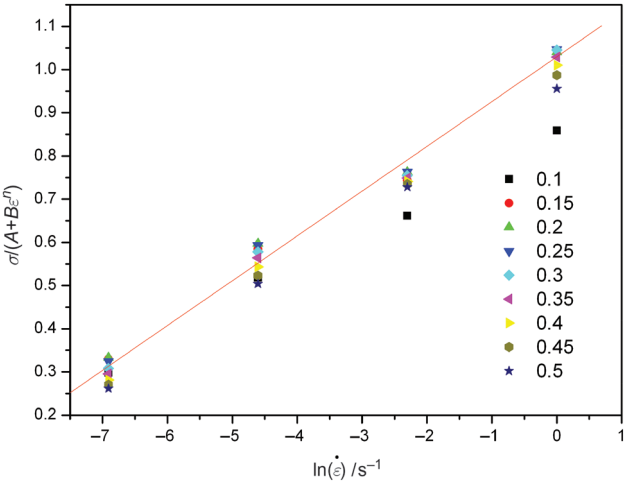

Figure 3: Relationship between $\sigma/A + B\varepsilon^n$ and $\ln(\dot{\varepsilon}^*)$ at the temperature of 1,073 K.

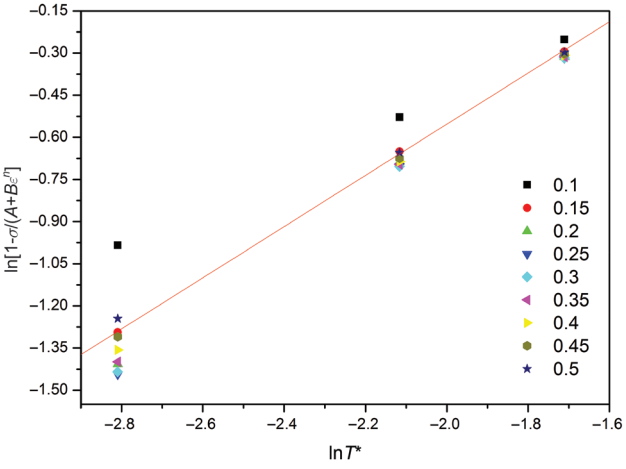

Figure 4: Relationship between $\ln[1 - \sigma/(A + B\varepsilon^n)]$ and $\ln T^*$.

Table 2: Parameters for the Johnson Cook model.

Parameter	*A*	*B*	*C*	*n*	*m*
Value	276.53	1.2162	0.09847	−1.8821	0.9279

The material constants of the Johnson Cook model for Ti–6Al–4V alloy are provided in Table 2. Then the Johnson Cook constitutive equation for Ti–6Al–4V alloy can be obtained:

$$\sigma = (276.53 + 1.2162\varepsilon^{-1.8821})(1 + 0.09847\ln\dot{\varepsilon}^*)(1 - T^{*0.9279}) \tag{6}$$

Using the constitutive equation above, the flow stress data for Ti–6Al–4V alloy are predicted at various processing conditions. Comparisons between the experimental and predicted data at various processing conditions using

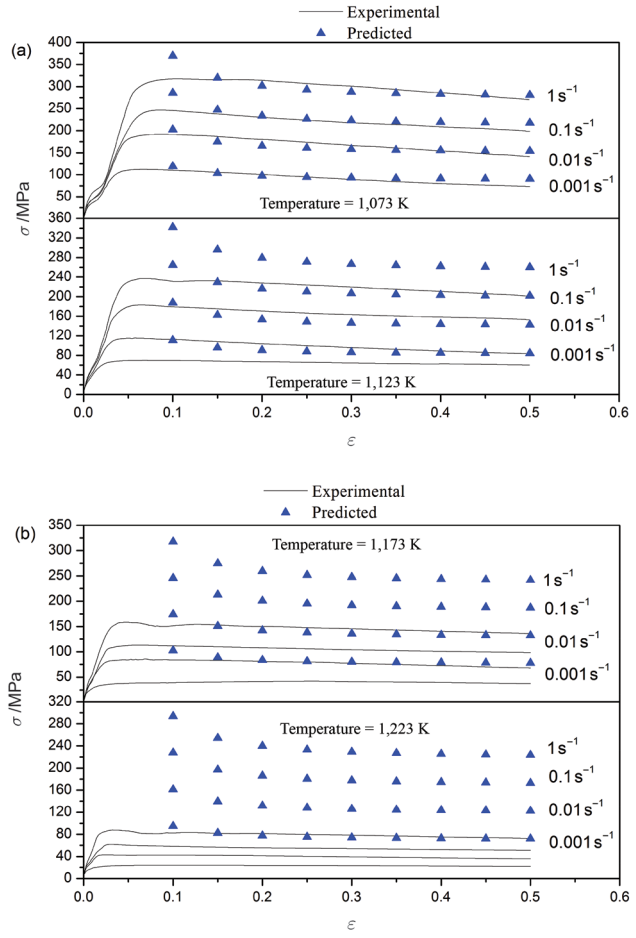

Figure 5: (a) Relationship between λ and $\ln \dot{\varepsilon}^*$. (b) Comparison between experimental flow stress and predicted flow stress using Johnson Cook model at the temperatures of (a) 1,073 and 1,123 K; (b) 1,173 and 1,223 K.

eq. (6) are shown in Figure 5. From Figure 5, it can be seen that the predicted flow stresses show a significant deviation in most of the loading conditions. Only at the temperature of 1,073 K, the predicted flow stress data from the Johnson Cook constitutive equation could track the experimental data of Ti–6Al–4V alloy.

Modified ZA model

The modified ZA constitutive model has been used to predict the flow stress behavior of materials at high temperatures as follows [24]:

$$\sigma = (C_1 + C_2\varepsilon^n)\exp[-(C_3 + C_4\varepsilon)T^* + (C_5 + C_6T^*)\ln\dot{\varepsilon}^*] \quad (7)$$

where $\dot{\varepsilon}^* = \dot{\varepsilon}/\dot{\varepsilon}_0$ is the dimensionless strain rate, $\dot{\varepsilon}_0$ the reference strain rat in s^{-1}, $T^* = T - T_{ref}$ and T_{ref} are the current and reference temperatures (K), respectively. C_1, C_2, C_3, C_4, C_5, C_6 and n are the materials constants. Like Johnson Cook model, here also 1,073 K is taken as reference temperature and 1 s^{-1} the reference strain rate. The corresponding procedure of evaluating the material constants is described as follows.

According to eq. (7), the following expression could be obtained at $\dot{\varepsilon}^* = 1$.

$$\sigma = (C_1 + C_2\varepsilon^n)\exp[-(C_3 + C_4\varepsilon)T^*] \quad (8)$$

Then taking natural logarithms of both sides of eq. (8), eq. (8) could be expressed as

$$\ln\sigma = \ln(C_1 + C_2\varepsilon^n) - (C_3 + C_4\varepsilon)T^* \quad (9)$$

Substituting the experimental flow stress data at $\dot{\varepsilon}^* = 1$ into eq. (9), the relationship between $\ln\sigma$ and T^* can be obtained (shown in Figure 6). Then, the values of $\ln(C_1 + C_2\varepsilon^n)$ and $-(C_3 + C_4\varepsilon)$ can be obtained from the intercept l_1 and slope S_1 of the line in the plot, respectively. Hence,

$$l_1 = \ln(C_1 + C_2\varepsilon^n) \quad (10)$$

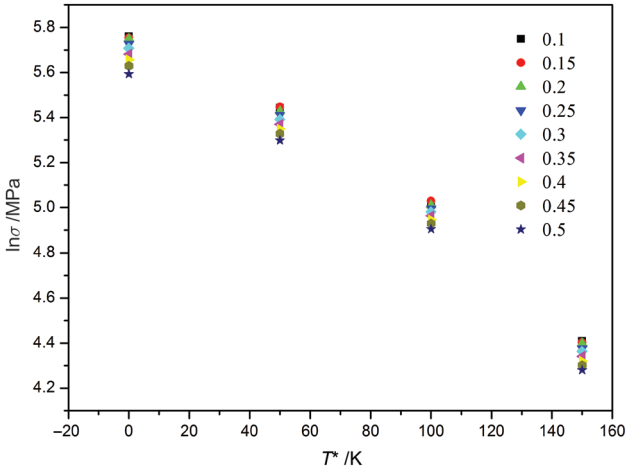

Figure 6: Plot of $\ln\sigma$ versus T^* at the reference strain rate.

After rearranging the equation above, eq. (10) can be derived as follows:

$$\ln(\exp l_1 - C_1) = \ln C_2 + n\ln\varepsilon \quad (11)$$

C_1 is determined from the yield stress of stress–strain curve at T = 1,073 K and $\dot{\varepsilon}^* = 1$. Substituting C_1 in eq. (10) and plotting the $\ln(\exp l_1 - C_1)$ versus $\ln\varepsilon$ graph the C_2 and n can be calculated, as shown in Figure 7. Similarly, the slope of the line represented by eq. (11) can be written as

$$S_1 = -(C_3 + C_4\varepsilon) \quad (12)$$

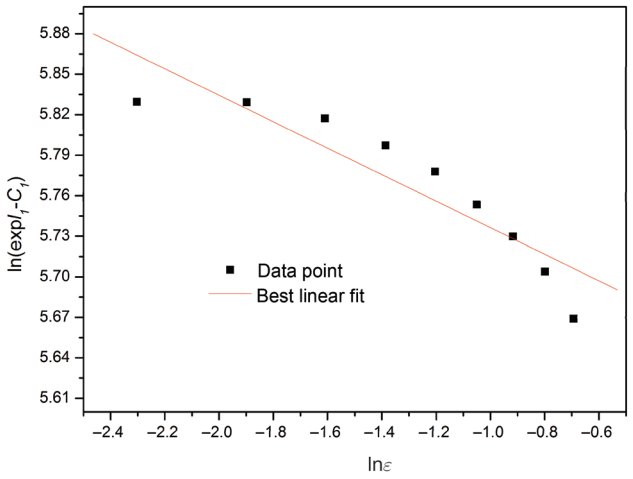

Figure 7: Relationship between $\ln(\exp l_1 - C_1)$ and $\ln \varepsilon$.

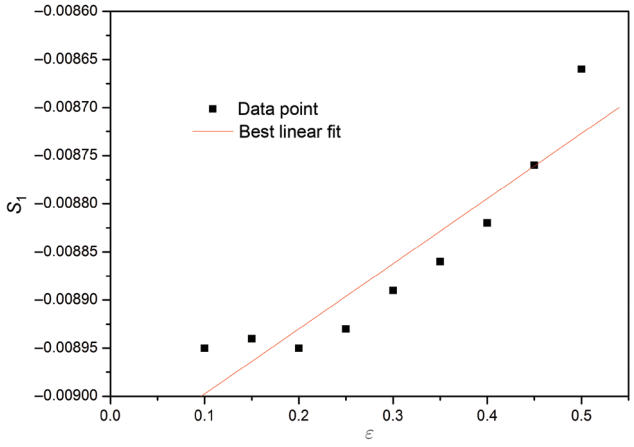

Figure 8: Relationship between S_1 and ε.

Therefore, C_i and C_4 can be easily obtained from the intercept and slope in the plot of S_1 versus ε, respectively, as can been seen from Figure 8. Then taking the natural logarithms of both sides of eq. (7), the following expression can be derived:

$$\ln \sigma = \ln(C_1 + C_2\varepsilon^n) - (C_3 + C_4\varepsilon)T^* + (C_5 + C_6T^*)\ln \dot{\varepsilon}^* \quad (13)$$

As can be seen from eq. (13), the $\ln \sigma$ versus $\ln \dot{\varepsilon}^*$ curve plot gives the value of $(C_5 + C_6T^*)$ as the slope S_2. Thus, a group of slope values under 5 different temperatures and 11 different strains were obtained. For four different temperatures, four different values of S_2 can be obtained at a specific strain, and the slope S_2 can be expressed as follows:

$$S_2 = C_5 + C_6T^* \quad (14)$$

Then, the values of C_5 and C_6 can be obtained from the intercept and slope of the S_2 versus T^* plot, respectively. Nine sets of C_5 and C_6 can be obtained at eight different strains as shown in Figure 9.

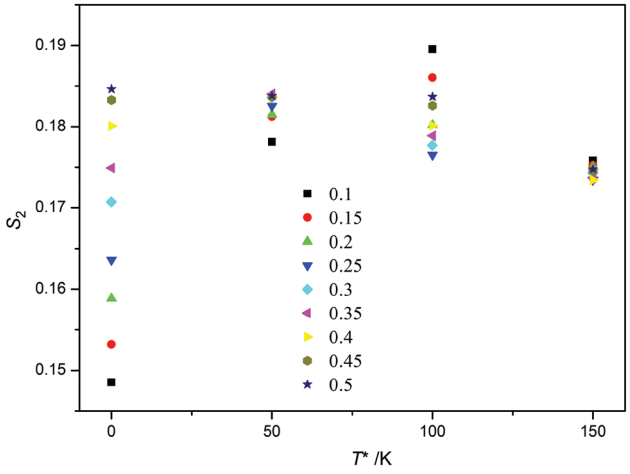

Figure 9: Plot of S_2 versus T^* at nine different strains.

In order to further verify the values of C_5 and C_6, the standard statistical parameter AARE was introduced. AARE is an unbiased statistical parameter for measuring predictability, and can be obtained through a term-by-term comparison of the relative error [14]:

$$\mathrm{AARE}(\%) = \frac{1}{N}\sum_{i=1}^{N}\left|\frac{E_i - P_i}{E_i}\right| \times 100 \quad (15)$$

where E and P are the experimental and predicted flow stresses, respectively, and N is the number of data employed in the investigation.

Substituting the nine sets of C_5 and C_6 values into the modified ZA model, the nine corresponding AARE values can be accordingly obtained. Based on the calculation results, the optimized values of C_5 and C_6 can be determined, as shown in Figure 10. The minimum AARE is

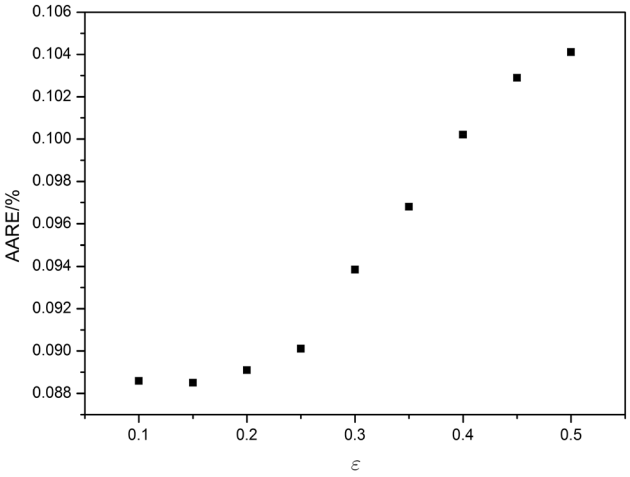

Figure 10: Values of the AARE derived using different groups of C_5 and C_6 at nine different strains.

Table 3: Parameters for the modified ZA model.

Parameter	C_1	C_1	C_2	C_4	C_5	C_6	n
Value	276.53	13.104	0.00907	−0.00068	0.1633	0.000142	−0.83365

8.85% and the optimized values of C_5 and C_6 are 0.1633 and 0.000142, respectively, at a strain of 0.15. Then the material constants involved in the modified ZA model can be determined, as shown in Table 3.

Therefore, the modified ZA model could be obtained as follows:

$$\sigma = (276.53 + 13.104\varepsilon^n)\exp[-(0.00907 - 0.00068\varepsilon)T^* + (0.1633 + 0.000142T^*)\ln\dot{\varepsilon}^*] \tag{16}$$

Using the constitutive equation above, the flow stress data can predicted for various deformation conditions. Comparison between the experimental and predicted values by modified ZA model at various processing conditions is shown in Figure 11. It can be seen in figure that there is a good agreement between the experimental and predicted values. In some deformation conditions (i.e. at 1,123 K in 0.1 s^{-1}, 1,173 K in 1 s^{-1}), an obvious variation between experimental and computed flow stress data could be observed.

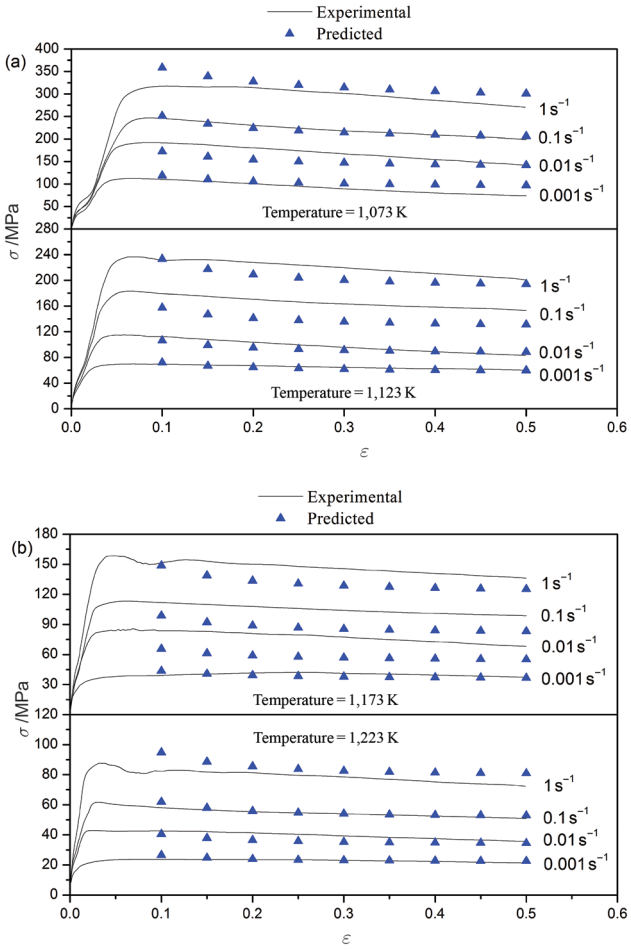

Figure 11: Comparison between experimental flow stress and predicted flow stress using modified ZA model at the temperatures of (a) 1,073 and 1,123 K; (b) 1,173 and 1,223 K.

Arrhenius-type model

The Arrhenius equation is widely employed to describe the correlation between strain rate, deformation temperature and flow stress, especially at elevated temperature [25]. Moreover, the effects of the temperature and strain rate on the deformation behaviors can be characterized by Zener–Hollomon parameter in an exponential equation as follows:

$$Z = \dot{\varepsilon}\exp\left(\frac{Q}{RT}\right) \tag{17}$$

$$\dot{\varepsilon} = AF(\sigma)\exp\left(-\frac{Q}{RT}\right) \tag{18}$$

$$F(\sigma) = \begin{cases} \sigma^{n'} & \alpha\sigma < 0.8 \\ \exp(\beta\sigma) & \alpha\sigma > 1.2 \\ [\sinh(\alpha\sigma)]^n & \text{for all } \sigma \end{cases} \tag{19}$$

where R is the universal gas constant (8.314 $J{\cdot}mol^{-1}{\cdot}K^{-1}$), d Q is the activation energy of hot deformation ($J{\cdot}mol^{-1}$), A, n', β, α and n are the materials constants. And

$$\alpha = \beta/n' \tag{20}$$

It can be seen that the effect of strain on the flow stress is not considered in eqs (17) and (18). However, the effect of the strain on the material constants is clear, and it influences the predictability of the constitutive model strongly. The following study on the Arrhenius-type model is based on the compensation of the strain effect. The strain of 0.3 is taken as an example to introduce the solution procedures of the material constants. For low as well as high stress levels, substituting Z and $F(\sigma)$ into eq. (18), respectively, then:

$$\dot{\varepsilon} = B\sigma^{n'} \tag{21}$$

$$\dot{\varepsilon} = C\exp(\beta\sigma) \tag{22}$$

where B and C are the material constants.

Then taking logarithm of both sides of eqs (21) and (22), the following equations can be obtained:

$$\ln(\sigma) = \frac{1}{n'}\ln(\dot{\varepsilon}) - \frac{1}{n'}\ln(B) \tag{23}$$

$$\sigma = \frac{1}{\beta}\ln(\dot{\varepsilon}) - \frac{1}{\beta}\ln(C) \tag{24}$$

The values of n' and β can be obtained from the slope of the lines in $\ln(\sigma) - \ln(\dot{\varepsilon})$ plot and $\sigma - \ln(\dot{\varepsilon})$ plot, as shown in Figure 12. Then, the corresponding value of $\alpha = \beta/n'$ can be obtained.

For low as well as high stress levels, eq. (18) can be written as follows:

$$\dot{\varepsilon} = A[\sinh(a\sigma)]^n \exp\left(-\frac{Q}{RT}\right) \tag{25}$$

Taking the logarithm of both sides of eq. (25) yields:

$$\ln[\sinh(\alpha\sigma)] = \frac{\ln\dot{\varepsilon}}{n} + \frac{Q}{nRT} - \frac{\ln A}{n} \tag{26}$$

For a particular temperature, differentiating eq. (26) gives

$$\frac{1}{n} = \frac{d\{\ln[\sinh(\alpha\sigma)]\}}{d(\ln\dot{\varepsilon})} \tag{27}$$

The value of n can be derived from the slopes of the lines of $\ln[\sinh(\alpha\sigma)] - \ln\dot{\varepsilon}$, as shown in Figure 13(a). The value of n is determined by averaging the values of n under different temperatures.

For a given strain rate, differentiating eq. (26) yields:

$$Q = Rn\frac{d\{\ln[\sinh(\alpha\sigma)]\}}{d(1/T)} \tag{28}$$

The value of Q can be obtained from the slopes in the plot of $\ln[\sinh(\alpha\sigma)] - 1/T$, as illustrated in Figure 13(b). The

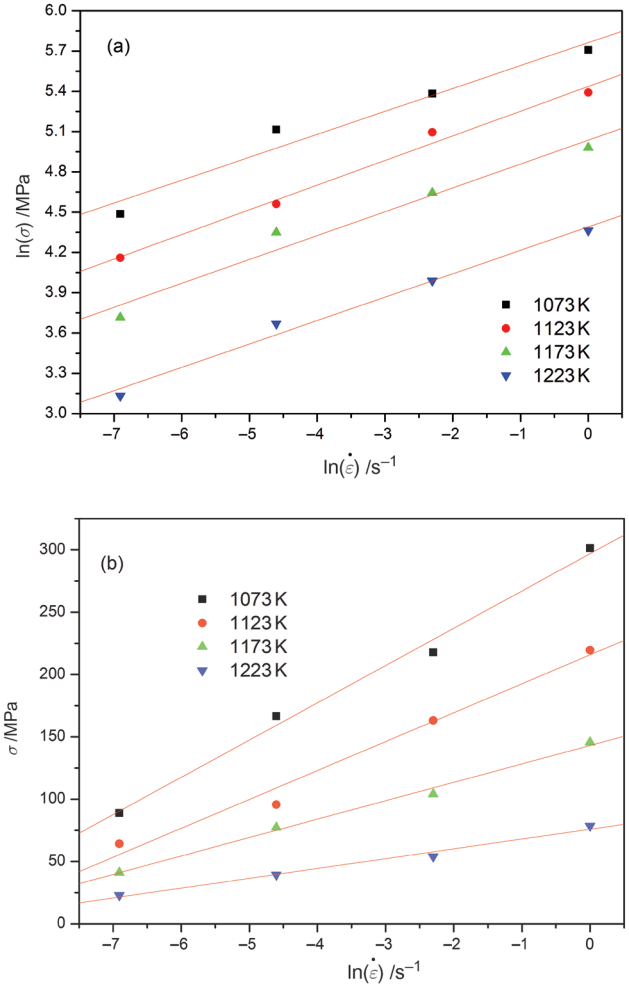

Figure 12: Relationship between (a) $\ln(\sigma)$ and $\ln(\dot{\varepsilon})$; (b) σ and $\ln(\dot{\varepsilon})$.

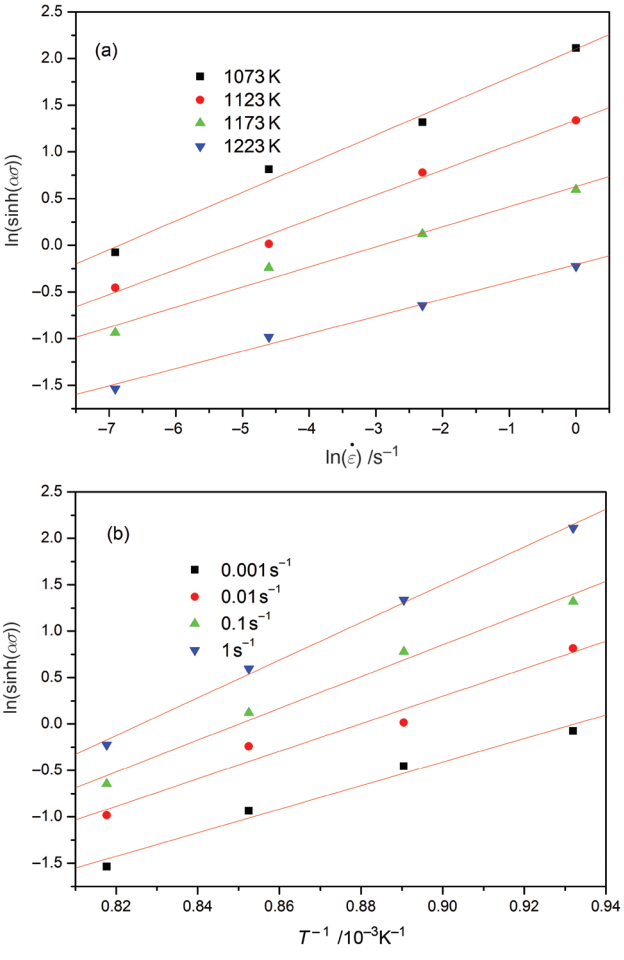

Figure 13: Relationship between (a) $\ln[\sinh(\alpha\sigma)]$ and $\ln(\dot{\varepsilon})$; (b) $\ln[\sinh(\alpha\sigma)]$ and $1/T$.

value of Q can be determined by averaging the values of Q under different strain rates. The values of A at a particular strain can be derived from the intercept of $\ln[\sinh(\alpha\sigma)]$–$\ln\dot{\varepsilon}$ plot.

The effect of strain on the material constants (i.e. α, n, Q and $\ln A$) is significant in the entire strain range, as shown in Figure 14. Therefore, the compensation of the strain should be taken into account to study the constitutive model more accurately. In this study, the influence of strain in the constitutive equation is incorporated by assuming that the material constants (i.e. α, n, Q and $\ln A$) are polynomial function of strains. As shown in eq. (29), a third order polynomial was found to represent the influence of strain on material constants with a good correlation and generalization, as shown in Figure 14. The polynomial fitting results of α, n, Q and $\ln A$ of Ti– 6Al–4V alloy are provided in Table 4:

$$\begin{aligned} \alpha &= C_0 + C_1\varepsilon + C_2\varepsilon^2 + C_3\varepsilon^3 \\ n &= D_0 + D_1\varepsilon + D_2\varepsilon^2 + D_3\varepsilon^3 \\ Q &= E_0 + E_1\varepsilon + E_2\varepsilon^2 + E_3\varepsilon^3 \\ \ln A &= F_0 + F_1\varepsilon + F_2\varepsilon^2 + F_3\varepsilon^3 \end{aligned} \tag{29}$$

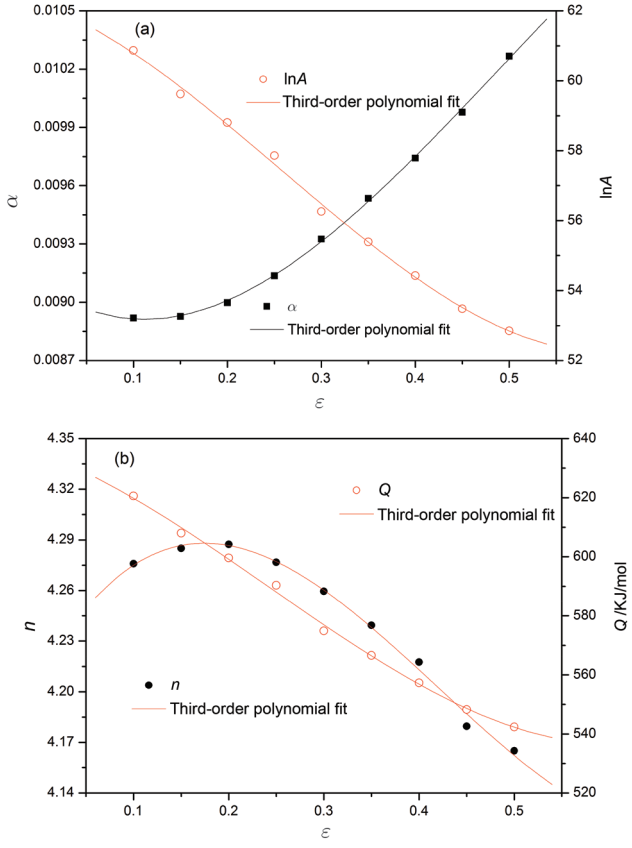

Figure 14: Variation of (a) α and $\ln A$; (b) n and Q with true strain.

Table 4: Coefficients of the polynomial for α, n, Q and $\ln A$.

α	n	Q	$\ln A$
$C_0 = 0.0091$	$D_0 = 4.2048$	$E_0 = 635.5309$	$F_0 = 62.2176$
$C_1 = -0.00346$	$D_1 = 1.0452$	$E_1 = -120.0112$	$F_1 = -9.82514$
$C_2 = 0.01748$	$D_2 = -3.7734$	$E_2 = -426.7681$	$F_2 = -50.7535$
$C_3 = -0.01185$	$D_3 = -3.0259$	$E_3 = 587.247$	$F_3 = 65.776$

Once the materials constants are evaluated, the flow stress at a particular strain can be predicted from following equation. Using the hyperbolic sine function, the constitutive equation relating the flow stress and Zener–Holloman parameter can be expressed in the following form:

$$\sigma = \frac{1}{\alpha}\ln\left\{\left(\frac{Z}{A}\right)^{1/n} + \left[\left(\frac{Z}{A}\right)^{2/n} + 1\right]^{1/2}\right\} \tag{30}$$

Comparison between the experimental and predicted values by strain-compensated Arrhenius-type constitutive equation at various processing conditions is shown in Figure 15. It can be seen from Figure 15 that there is a good agreement between the experimental and predicted values except at the temperature of 1,173 K in 0.001 s^{-1} and 1,223 K in 1 s^{-1}.

Discussion

The Johnson Cook model shows good prediction only at reference temperature. Similar results were reported by Samantaray [12] and He [26] in 9Cr–1Mo steel and 20CrMo alloy steel respectively. This may be accounted for the fact that the Johnson Cook model considers only the yield and strain hardening portion without considering the coupled effects of the temperature and strain rate on the flow behaviors [9].

It can be seen from Figure 9 that the relationship between S_2 and T^* is obviously nonlinear. However, the modified ZA model also shows good prediction of the elevated temperature flow behavior of the Ti–6Al–4V alloy except under some deformation conditions, as can be seen in Figure 11. The reason is not quite clear to us. Possibly, the values of S_2 vary in a small range, as shown in Figure 12(a) (when $\dot{\varepsilon}_0 = 1$, $\dot{\varepsilon}^* = \dot{\varepsilon}$, and $\ln\sigma$ vs $\ln\dot{\varepsilon}$ can be regarded as $\ln\sigma$ vs $\ln\dot{\varepsilon}$). Then the variation in the

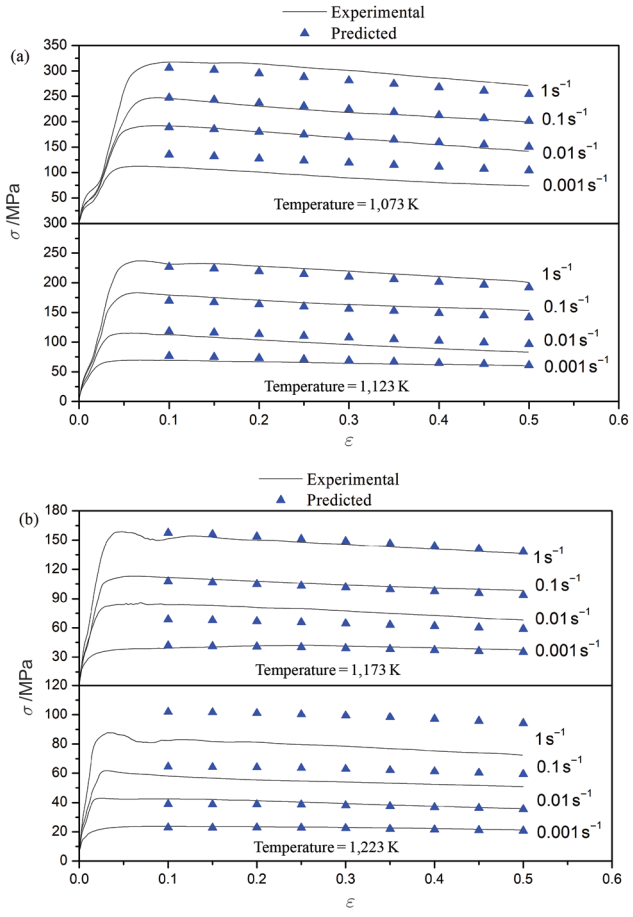

Figure 15: Comparison between the experimental and predicted flow stress by strain-compensated Arrhenius-type equation at the temperature (a) 1,073 and 1,123 K; (b) 1,173 and 1,223 K.

slope of the S_2 versus T^* lines may be attributed to little scattering in the predicted flow stress data. Compared with these two models, the strain-compensated Arrhenius-type constitutive model could predict the flow stress more accurately at the temperature of 1,123 and 1,173 K, as shown in Figure 15. However, a remarkable variation between experimental and computed flow stress data can be observed at the temperature 1,223 K in 1 s^{-1}. Similar observation has been made by Ji [7] and Mandal [14] in Aermet100 steel and Ti-modified austenitic stainless steel at higher strain rate. Meanwhile, all the results obtained from the three kind of developed models exist obvious variation in some deformation conditions, as shown in Figures 5, 11 and 15. This may because the response of deformation behaviors of the materials under elevated temperatures and strain rates is highly nonlinear, and many factors affecting the flow stress are also nonlinear, which make the prediction accuracy of the flow stress by the constitutive equations low and the applicable range limited [27].

The accuracy of the above-mentioned models is quantified in terms of correlation coefficient (R) and AARE. R is expressed as following equations [28]:

$$R = \frac{\sum_{i=1}^{N}(E_i - \bar{E})(P_i - \bar{P})}{\sqrt{\sum_{i=1}^{N}(E_i - \bar{E})^2 \sum_{i=1}^{N}(P_i - \bar{P})^2}} \tag{31}$$

where E is the experimental flow stress (MPa) and P is the predicted flow stress (MPa) obtained from the developed constitutive equation. $\bar{E}$ and $\bar{P}$ are the mean values of E and P, respectively. N is the total number of data used in this study. Correlation coefficient R is a commonly used statistical parameter and can provide information on the strength of the linear relationship between the experimental and predicted data.

The comparisons between experimental flow stresses and predicted data by the three developed models are shown in Figure 16. It can be seen from figures that most of the data points locate close to the fitting lines, and the values of R for Johnson Cook, modified ZA and strain-compensated Arrhenius-type constitutive models are 0.790, 0.994 and 0.989, respectively. The values of AARE for the Johnson Cook, modified ZA and strain-compensated Arrhenius-type constitutive models are 91.66%, 8.85% and 9.13%, respectively. Based on the calculation procedure described above, it can be determined that modified ZA model and the strain-compensated Arrhenius-type model could predict the elevated temperature flow stress behavior for Ti–6Al–4V titanium alloy in α + β phase region, while the Johnson Cook could not track the experimental data. The value of AARE of strain-compensated Arrhenius-type model is a little larger than that of the modified ZA model. Meanwhile, it can be found that the number of material constants involved in the strain-compensated Arrhenius-type model was 24. In contrast, only five and seven material constants are involved in the Johnson Cook as well as the modified ZA model, respectively. And the time required for evaluating these material constants of the strain-compensated Arrhenius-type constitutive equation is also much longer than that of the other two models. This proves that the modified ZA model produce reasonable results more efficiently with fewer material constants.

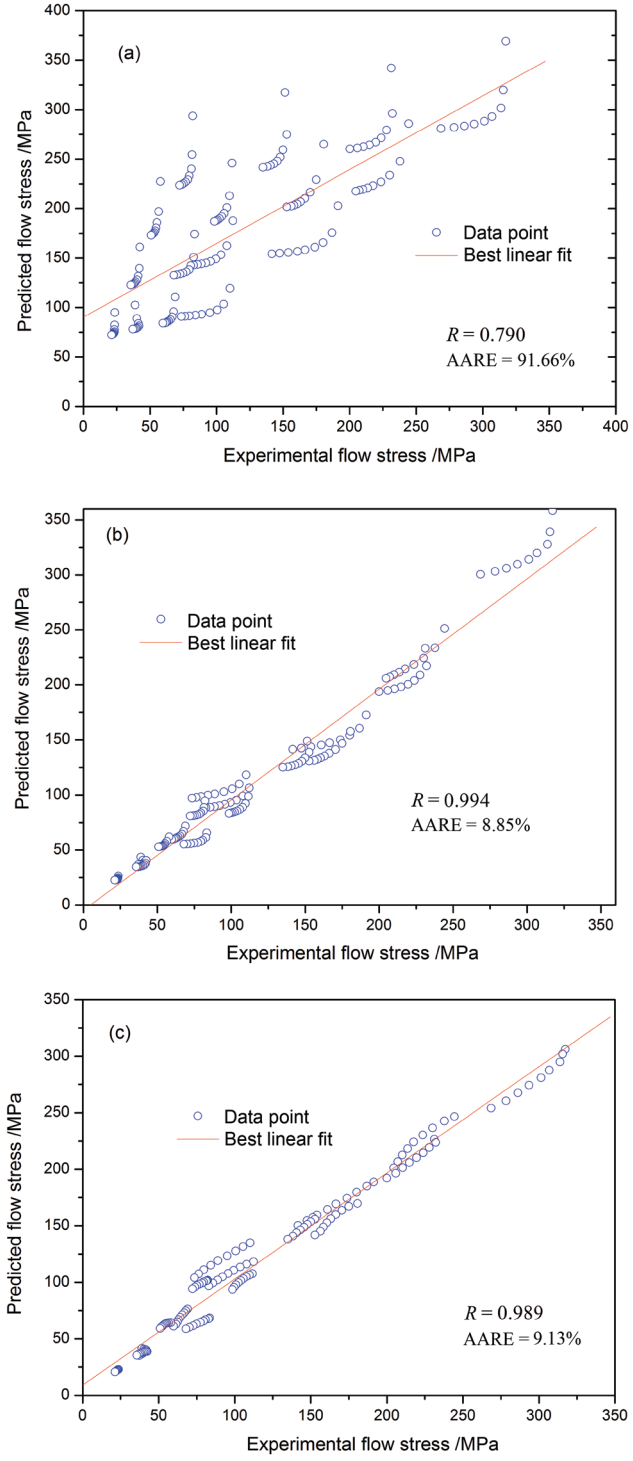

Figure 16: Correlation between the experimental and predicted flow stress values from (a) modified Johnson Cook model (b) modified ZA model; and (c) the strain-compensated Arrhenius-type model.

Conclusions

A comparative study has been made on the ability of the Johnson Cook, modified ZA and strain-compensated Arrhenius-type constitutive models to describe the high-temperature flow behavior of Ti–6Al–4V titanium alloy in the temperature range of 1,073–1,223 K with the strain rate of 0.001–1 s^{-1}. Based on this study, the following conclusions can be drawn:

(1) The Johnson Cook is inadequate to predict high-temperature flow behavior of Ti–6Al–4V alloy over the entire range of strain rates, temperatures and strains, while modified ZA and strain-compensated Arrhenius-type models could predict the flow stress behavior of Ti–6Al–4V alloy at elevated temperatures well.

(2) The predictability of three developed constitutive equation models was quantified in terms of correlation coefficient (R) and AARE. It was found that the values of AARE from the Johnson Cook, modified ZA and strain-compensated Arrhenius-type models are 99.66%, 8.85% and 9.13%, respectively, and the correlation coefficients are 0.790, 0.994 and 0.989 correspondingly, which indicated that the modified ZA-type constitutive equation could represent the elevated temperature flow behavior more accurately in the entire processing domain.

(3) The Johnson Cook and modified ZA constitutive models involve only five and seven material constants, respectively, and the time required for evaluating these material constants involved in the two models also much shorter than that of strain-compensated Arrhenius-type constitutive model.

Funding: The authors gratefully acknowledge the financial support received from Natural Science Foundation of Shaanxi Province (2014JM6230), Innovation Team Project of "Processing and Preparation for High-performance Non-ferrous Metal Materials" of Xi'an University of Architecture and Technology, Fundamental Science Funds of Xi'an University of Architecture and Technology (JC1308) and Talents Science Fund of Xi'an University of Architecture and Technology (RC1369).

References

[1] H.Y. Li Y.H. Li, D.D. Wei, J.J. Liu and X.F. Wang, Mater. Sci. Eng. A., 530 (2011) 367–372.
[2] P. Changizian, A. Zarei-Hanzaki and A. Roostaei, Mater. Des., 39 (2012) 384–389
[3] C. Li, M. Wang, .X.D. Wu and H. Lin, Mater. Sci. Eng. A., 527 (2010) 3623–3629.
[4] Y. Han, G.J. Qiao, J.P. Sun and D.N. Zou, Comput. Mater. Sci., 67 (2013) 93–103.
[5] D. Samantaray, S. Mandal and A.K. Bhaduri, Mater. Des., 31 (2010) 981–984.

[6] Y.H. Xiao and C. Gao, Mater. Sci. Eng. A., 528 (2011) 5081–5087.
[7] G.L. Ji, F.G. Li, Q.H. Li, H.Q. Li and Z. Li, Mater. Sci. Eng. A., 528 (2011) 4774–4782.
[8] A. Abbasi-Bani, A. Zarei-Hanzaki, M.H. Pishbin and N. Haghdadi, Mech. Mater., 71 (2014) 52–61.
[9] H.Y. Li, Y.H. Lia, X.F. Wang, J.J. Liu and Y. Wu, Mater. Des., 49 (2013) 493–501.
[10] S.T. Chiou, W.C. Cheng, and W.S. Lee, Mater. Sci. Eng. A., 329 (2005) 156–162.
[11] W.S. Lee and C.Y. Liu, Mater. Sci. Eng. A., 426 (2006) 101–113.
[12] D. Samantaray, S. Mandal and A.K. Bhaduri, Comput. Mater. Sci., 47 (2009) 568–576.
[13] H.J. Zhang, W.D. Wen and H.T. Cui, Mater. Sci. Eng. A., 527 (2009) 328–333.
[14] S. Mandal, V. Rakesh, P.V. Sivaprasad, S. Venugopal and K.V. Kasiviswanathan, Mater. Sci. Eng. A., 500 (2009) 114–121.
[15] J. Li, F.G. Li, J. Cai, R.T. Wang, Z.W. Yuan and F.M. Xue, Mater. Des., 42 (2012) 369–377.
[16] C.H. Liao, H.Y. Wu, S.H. Lee, F.J. Zhu, H.C. Liu and C.T. Wu, Mater. Sci. Eng. A., 565 (2013) 1–8.
[17] S. Bruschi, S. Poggio, F. Quadrini and M.E. Tata, Mater. Lett., 58 (2004) 3622–3629.
[18] C.S. Lee, S.B. Lee, J.S. Kim and Y.W. Chang, Int. J. Mech. Sci., 42 (2000) 1555–1569.
[19] J. Luo, M.Q. Li, H. Li and W.X. Yu, Chin. J. Nonferrous Met., 18 (2008) 1395–1401.
[20] F. Warchomicka, C. Poletti, M. Stockinger and T. Henke, Int. J. Mater. Form., 3 (2010) 215–218.
[21] S.H. Huang, Y.Y. Zong and D.B. Shan, Mater. Sci. Eng. A., 561 (2013) 17–25.
[22] Y.C. Zhu, W.D. Zeng, X. Ma, Q.A. Tai and X.G. Li, Tribol. Int., 44 (2011) 2074–2080.
[23] G.R. Johnson and W.H. Cook, Proceedings of the Seventh International Symposium on Ballistics. International Ballistics Committee, Hague (1983), pp. 541–547.
[24] D. Samantaray, S. Mandal, A.K. Bhaduri, S. Venugopal and P.V. Sivaprasad, Mater. Sci. Eng. A., 528 (2011) 1937–1943.
[25] C.M Sellars and W.J. Mctegart, Acta Metall., 14 (1966) 1136–1138.
[26] A. He, G.L. Xie, H.L. Zhang and X.T. Wang, Mater. Des., 52 (2013) 667–685.
[27] Y.C. Lin, J. Zhang and J. Zhong, Comput. Mater. Sci., 43 (2008) 752–758.
[28] M.P. Phaniraj and A.K. Lahiri, J. Mater. Process. Technol., 141 (2003) 219–227.